

Batch removal of aqueous nitrate ions using an effective nano-biocomposite

Sepehri S.*and Nakhjavanimoghaddam M.M.

Agricultural Engineering Research Institute (AERI), Agricultural Research, Education and Extension Organization (AREEO), P.O. Box 31585-845, Karaj, Iran

Received: 15/08/2018, Accepted: 16/10/2018, Available online: 25/10/2018

*to whom all correspondence should be addressed: e-mail: s.sepehri@aeri.ir, sepehri_saloom@yahoo.com

<https://doi.org/10.30955/gnj.002868>

Abstract

The intent of this research is the investigation of the nitrate reduction from aqueous solution using biomass (pine cone (PC) and PC activated carbon (PCAC)) – supported zero valent iron nanoparticles (PC-Fe⁰ and PCAC-Fe⁰). The synthesis of these nano-bio-composites was based on the reduction of ferrous iron with borohydride, in which PC and PCAC acted as porous-based support materials. The structure of the adsorbents was characterized by SEM, XRD, FTIR and BET analysis. The SEM images revealed that nZVI immobilized on PC-Fe⁰ and PCAC-Fe⁰ were spherical and uniformly dispersed on the surface of the stabilizers. Batch experiments indicated that the nitrate removal efficiency decreased with the increase in the initial nitrate concentration and initial pH, but increased with the increase in the sorbent dosage and temperature. The maximum adsorption capacities of PC-Fe⁰ and PCAC-Fe⁰ for nitrate were 18.16 and 22.30 (mg/g), respectively. The nitrogen mass balance calculations revealed that zero valent iron nanoparticles in both PC-Fe⁰ and PCAC-Fe⁰ beads could generally reduce nitrate into ammonium, and nitrite usually was occurred as intermediate. Subsequently, PCAC-Fe⁰ absorbs completely un-wanted ammonium, while PC-Fe⁰ releases little ammonium in the solution.

Keywords: Bio activated carbon; kinetic modeling; nanoscale zero-valent iron particles; redox reaction; sorption isotherm.

1. Introduction

High nitrate concentration has become a serious common water quality problem in agricultural regions. The sources of nitrogen compounds accumulation in the environment include industrial wastewaters and municipal discharges, nitrogenous fertilizers, the unreasonable disposal of animal wastes, septic systems, and atmospheric deposition from nitrogen oxide emission (Driscoll *et al.*, 2003). The nitrate has high chemical stability, especially at low concentrations, which can cause environmental problems, such as, eutrophication. In addition, groundwater is a considerable source of drinking water.

Continuous uptake of nitrate and nitrite via drinking water will lead to several health treats to human including, cancers and methemoglobinemia (Kim *et al.*, 2015). Many technologies are available for treating nitrate from water, such as, ion exchange, reverse osmosis, adsorption, biological and chemical reductions (Tada *et al.*, 2004). Although, these techniques are effective in removing nitrate from water, most of them are limited in the factual application for the remediation.

In recent years, nanoscale Zero-Valent Iron (nZVI) particles has been widely studied as an environmentally friendly strong reducing agent. Due to its small size, high specific surface area, suitable redox potentials and faster and more complete reactions (comparison with other ZVI materials), nZVI (nZVI<100 nm) is a promising alternative for water contaminants removal (Mukherjee *et al.*, 2016). Several studies reported the efficiency of nZVI for the removal of a variety of contaminants including heavy metals (Hou *et al.*, 2008), aromatic compounds (Lomnicki and Dellinger, 2003), pesticides (Joo and Zhao, 2008) and dyes (Lin *et al.*, 2008). However, iron nanoparticles expose vigorous propensity to agglomerate into micron or larger solid particles. This is unavoidable because of the high surface energy, intrinsic magnetic interaction and direct interparticle interactions, such as, van der waals forces. Furthermore, the separation of non-supported iron nanoparticles from the aqueous phase is still a difficult undesirable task (Wang *et al.*, 2008). Agglomeration reduces the effective surface area and thereby decreasing both particle reactivity and removal efficiency (Pan *et al.*, 2010). Recently, iron nanoparticles have been modified to prevent their aggregation and improve their removal abilities, such as, mechanical strength, stability, reactivity and flexibility (Zhao *et al.*, 2016). It was reported that the chemical reduction of an aqueous iron salt with borohydride in the presence of porous supporting materials, can decrease the aggregation of iron nanoparticles (Shi *et al.*, 2011). This method has many advantages, such as, safety, facility, cost-effective, and simplicity. Nano-ZVI stabilization on supporting material

allows direct contact with the contaminant, reduces the electron path from the nano-ZVI to the target contaminant and increases nano-ZVI reactivity (Bossa *et al.*, 2017). To prevent the aggregation of nanoparticles, various stabilizers have been found effective for stabilizing nZVI including polymers (Li *et al.*, 2011a), nanostructure carbons and surfactant (Sun and Zeng, 2002). Huang *et al.* (2016) reported that sodium alginate (SA)-modified nanoscale zero-valent iron (NZVI), play a constructive role in the remediation of cadmium contaminated river sediments (Huang *et al.*, 2016). Nanoscale zero valent iron particles stabilized by epichlorohydrin/chitosan (ECH-CS-nZVI) beads have been reported to increase their dispersibility and stability. A removal rate of Cr (VI) using ECH-CS-nZVI beads could be maintained as high as 76.6% and 48.2% on the second and third runs, respectively, which hinted that ECH-CS-nZVI beads could be regenerated (Liu *et al.*, 2012). The study of Wang *et al.* (2015) suggested that hydroxyethyl cellulose and hydroxypropylmethyl cellulose dispersed NZVI can be utilized as a promising modified nano-material for degradation of dye wastewater (Wang *et al.*, 2015). Li *et al.* (2010) investigated Cr (VI) removal by Montmorillonite and hexadecyl trimethylammonium modified montmorillonite (HDTMA-Mont) supported iron nano-particles. They reported that the presence of organo-montmorillonite apparently decreased the extent of aggregation and the size of the iron particles. In contact with Cr(VI), the reduction of Cr(VI) was highest with HDTMA-Mont/iron particles, followed by Mont/iron particles and free iron nanoparticles (Li *et al.*, 2010). In another study, Shi *et al.* (2011) reported that bentonite-supported nanoscale zero-valent iron had a Specific Surface Area (SSA) of 39.94 (m² g⁻¹), while the SSAs of nZVI and bentonite were 54.04 and 6.03 (m² g⁻¹), respectively (Shi *et al.*, 2011).

In this research, natural materials, which are abundant and environmental-friendly, are used as the supporting materials of iron nanoparticles. Their sorption capacity attracts contaminants to the surface, and thus enhances the efficiency. So, pine cone (PC) and activated carbon prepared from pine cone (PCAC) were used as the supporting materials for nZVI and then, the removal of nitrate from aqueous solution was investigated using these modified sorbents (PC-Fe⁰ and PCAC-Fe⁰). This paper reports four issues as follows: (1) the synthesis of PC-Fe⁰ and PCAC-Fe⁰ by the reduction of Fe²⁺ ions with NaBH₄, and the characterization of the modified beads with Scanning Electron Microscopy (SEM), powder X-ray Diffraction (XRD), Fourier Transform Infrared spectroscopy (FTIR), and Brunauer–Emmett–Teller (BET-N₂) technology, (2) the comparison of nitrate removal by raw materials, PC-Fe⁰ and PCAC-Fe⁰, (3) the kinetics and isotherm of nitrate reduction by raw materials, PC-Fe⁰ and PCAC-Fe⁰, and finally, (4) the evaluation of the initial nitrate concentration, sorbent dosage, initial pH, and adsorption temperature effects on the removal process.

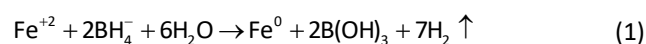
2. Experimental details

2.1. Materials and chemicals

In this study, all the chemicals were reagent grade, and distilled water was used in all preparations. All reagents were listed below, purchased from Merck or Aldrich: Ferrous sulfate heptahydrate (FeSO₄·7H₂O), sodium borohydride (NaBH₄), potassium nitrate (KNO₃), ethanol, NaOH, HCl, and phosphoric acid.

2.2. Preparation of PCAC, PC-Fe⁰, and PCAC-Fe⁰

PC was obtained from Tehran in Iran. After drying at 80°C for 24 h, PC was ground and sieved with a 200 mesh screen prior to use in the experiments. Powdered activated carbon was derived by thermal-chemical procedure from the ground PC. Raw materials were impregnated with 85wt.% H₃PO₄ solution in the weight ratio of 1:3. To produce activated carbon, acid impregnated samples were placed in an electrical heating furnace with inert atmosphere of nitrogen at a flow rate of 25 ml min⁻¹ and heated in two phases. In the first phase, the reactor was heated at a heating rate of 6°C min⁻¹ up to 170 °C and held at this temperature for 60 min. The second phase included heating with the rate of 8°C min⁻¹ up to 500 °C and 60 min retention at this temperature. After gradual cooling down to room temperature in a nitrogen gas stream overnight, the final product was repeatedly washed with hot DI water until the pH of rinsing water reached a value of 7. Finally, PCAC samples were dried at 110 °C for 24 h and stored in a desiccator for later use. The synthesis of PC-Fe⁰ and PCAC-Fe⁰ was performed according to the borohydride reduction method. In a typical synthesis of PC-Fe⁰ and PCAC-Fe⁰, a ferrous solution was first prepared by dissolving FeSO₄·7H₂O (iron/(bead) mass ratio 1:1) in a 4/1 (v/v) absolute ethanol/deionized water mixture (50 mL). The solution was placed into a three-necked open flask. The solution was mixed with 1 g PC and PCAC and stirred for 2 h. PC-Fe⁰ and PCAC-Fe⁰ were synthesized in the solution by reducing Fe (II) to Fe⁰ using NaBH₄ in the presence of PC and PCAC as stabilizers. Then, 55 mL of freshly prepared aqueous solution containing 2.04 g of NaBH₄ (BH₄⁻/Fe²⁺ molar ratio of 3.0) was added drop-wise into the mixture, while stirring continuously on a magnetic stirrer resulting in formation of black Fe⁰ nanoparticles and evolution of H₂. The whole process was carried out under inert gases flow of N₂ to avoid the oxidization of PC-Fe⁰ and PCAC-Fe⁰. The values of experimental parameters such as pH, reaction time, reactant concentrations, titration rate, temperature (25 ± 0.5 °C), and stirring speed, were maintained constant during the experiment (Uzum *et al.*, 2009). The borohydride reduces the Fe (II) to Fe⁰ according to the following reaction (Li *et al.*, 2010):



The formed suspension was filtered and the black PC-Fe⁰ and PCAC-Fe⁰ were washed three times with pure ethanol and dried overnight at 75°C under vacuum and kept under a N₂ atmosphere prior to use (Uzum *et al.*, 2009). Elemental analyses of PC were determined using a

Costech ECS 4010 Elemental Analyzer. Physical properties and compositions of PC and PCAC were determined according to the literatures. Morphologies and sizes of the particles were observed with SEM using a Hitachi S-4160, 20.0 kV. The SSAs of PC, PCAC, PC-Fe⁰ and PCAC-Fe⁰ samples were measured by the BET-N₂ method using a Belsorp mini II (BelJapan) instrument. A Philips X'PERTMPD diffractometer, equipped with a graphite-monochromatized (Cu-K α radiation, $\lambda=1.54$ Å) was used to obtain the XRD patterns. All samples were recorded (Haykiri *et al.*, 2010) between 10 and 70° (2 θ) at a scanning rate of 0.05°/s. The FTIR spectra of the samples were recorded as KBr pellets in the spectral range 500-4000 cm⁻¹ by a Tensor 27 (Bruker) FTIR spectrometer at room temperature. The concentrations of nitrate and nitrite in the solutions were analyzed based on the guidelines of the 20th edition of the standard methods by means of a UV-Vis spectrophotometer (V-530) (APHA, 1992). At the end of the reaction, the mass of ammonium sorbed on the PC-Fe⁰ and PCAC-Fe⁰ was measured by extracting with 1 M KCl solution and analyzing the extract solution. NH₄⁺ concentration in the solutions was analyzed by a steam distillation procedure (Keeney and Nelson, 1982). The pH of the solutions was adjusted using 0.1 M HCl/NaOH using a pH meter (Metrohm, 827 pH Lab).

2.3. Batch experiments

To evaluate the efficiency of produced materials for nitrate removal in the aqueous solution, experiments were conducted using PC, PCAC, PC-Fe⁰ and PCAC-Fe⁰. The aqueous nitrate solutions were prepared by dissolving appropriated amounts of KNO₃ in distilled deionized water. To determine the dependence of the removal efficiency on pH and temperature, the initial pH values of nitrate solutions and adsorption temperature were varied from 2 to 10 and 25 to 55 °C, respectively. The effect of the adsorbents dosage on nitrate removal efficiency was investigated by applying various amounts of adsorbents

Table 1. Characteristics of PC sample

Structural components (%)				
Cellulose	Holocellulosics	Lignin	Extractives	Ash
29.96	20.63	44.84	4.55	1.76
Physico-chemical characteristics (%)				
Ash	Carbon	Oxygen	Hydrogen	Nitrogen
1.76	39.65	48.63	7.74	2.11

Table 2. Physico-chemical characteristics of PCAC

Nitrogen (%)	Hydrogen (%)	Ash(%)	Carbon (%)
2.96	2.03	4.17	82.45
Oxygen (%)	Iodine number (mg g ⁻¹)	Bulk density (kg m ⁻³)	
8.12	780	450	

The morphology of PC and PCAC, and the distribution of nZVI particles on the surface of PC-Fe⁰ and PCAC-Fe⁰ before and after reaction with nitrate ions were analyzed using SEM (Figure 1a-1f). PC sample (Figure 1a) is angular, and the grains show non uniform shape with large

(2-10 g L⁻¹). Equilibrium isotherm studies were performed with different initial concentrations of nitrate from 20 to 320 (mg L⁻¹), while the initial pH of the solutions were fixed at the (6 ±0.1). The kinetic studies were carried out to determine the best fitted kinetic model and equilibrium time of the adsorption. The batch experiments were carried out in 50 ml polyethylene bottles containing 0.1 g sorbents and 10 mL of nitrate solutions of desired concentrations and pH at room temperature (25±1 °C). All adsorption tests were performed in triplicate. The solutions were mixed on a shaker with an agitation speed of 200 rpm at 25 °C. The samples were collected periodically. At the end of the adsorption period of 24 h, each sample was filtered and the nitrate concentration in the supernatant was analyzed immediately. The removal efficiency (Re%) and the adsorption capacity (q_e(mg g⁻¹)) of sorbents were calculated as follows:

$$Re(\%) = \frac{C_0 - C_e}{C_0} \times 100 \quad (2)$$

$$q_e = \frac{(C_0 - C_e) \times V}{m} \quad (3)$$

Where C₀, C_e (mg L⁻¹), m and V are the concentrations of nitrate at initial and equilibrium, the mass of sorbent (g), and the volume of the solution (L), respectively.

3. Results and discussion

3.1. Characterization of PC, PCAC, PC-Fe⁰, and PCAC-Fe⁰

The Physico-chemical characteristics and structural components of PC are presented in Table 1. Moreover, important properties of PCAC are summarized in Table 2. The SSAs of PC, PCAC, PC-Fe⁰, and PCAC-Fe⁰ measured by BET analysis were 6.1, 350.8, 52.2, and 870.6 (m² g⁻¹), respectively. Immobilization of zero-valent iron nanoparticles onto PC and PCAC were accompanied by a significant increase in the specific surface areas.

breakage including straight and arcuate steps and fractured plates. The SEM image of PCAC (Figure 1b) clearly shows that the adsorbent has porous surface, indicating relatively high surface area, and pores of different sizes and shapes can be observed. It can be seen (Figure 1c) that shape of the nZVI particles immobilized on PC-Fe⁰ is generally spherical. Measuring the diameters of 100 particles in different regions of a given image grid can be used to quantify the particle size (Wang *et al.*, 2010). In accordance to this method, the particles size ranged from 45 to 110 nm, with a mean particle diameter of 78 nm, and some aggregates are noted. In the case of PCAC-Fe⁰ (Figure 1d), stabilized nZVI particles have the core-shell structure, clearly discrete and uniformly dispersed on

the surface of the stabilizer without any obvious aggregation. The diameter of the particles ranged from 25 to 55 nm with an average size 40 nm. PCAC-Fe⁰ has smaller particle sizes than PC-Fe⁰; this might be attributed to the porous structure of the activated carbon. Fe²⁺ ions were adsorbed on the surface of the activated carbon, and generally situated at inside channel space. These ions were reduced to Fe⁰ with NaBH₄. Therefore, Fe⁰ ions were dispersed uniformly on the activated carbon surface. This observation is supported by BET surface area of the activated carbon. Similar results have been reported using bentonite and kaolinite supported iron nano particles, which were used to remove Cr (VI) and Co(II) from an aqueous solution, respectively (Shi *et al.*, 2011; Uzum *et al.*, 2009).

In contrast, as indicated in Figures 1e and 1f, the sizes of nZVI particles increase significantly after reacting with nitrate ions. These particles have nearly rectangular shape. This phenomena could be attributed to the formation of iron (hydr)oxides on the surface of the nanoparticles, occurred due to the redox reaction between immobilized nZVI particles and nitrate ions.

The XRD patterns of PC, PCAC, PC-Fe⁰ and PCAC-Fe⁰ before and after reacting with nitrate ions are shown in Figure 2. The XRD pattern of PC (Figure 2a), displayed the raw material has a less organized structure with no indication of any specific crystalline structure. The XRD pattern of PC-Fe⁰ shows apparent peaks of Fe⁰ (b2: 2 θ =44.67° and b3: 2 θ =65.03°) (Figure 2b). Moreover, this pattern indicates a weak reflection at 2 θ =33.88° (b1) corresponding to iron oxide (maghemite). The XRD pattern of PC-Fe⁰ after reaction with nitrate (Figure 2c) indicated the presence of lepidocrocite (c1: γ -FeO(OH), 2 θ =26.9), goethite (c2: α -FeOOH, 2 θ =36.6), magnetite (c3: Fe₃O₄, 2 θ =47.18) and maghemite (c4: γ -Fe₂O₃, 2 θ =60.68). Figure 2d reveals a peak at 2 θ =25° (d1) originated from the amorphous structure of carbon (Allaf *et al.*, 2011). According to the XRD results (Figure 2e), PCAC-Fe⁰ before reacting with nitrate ions contained no significant amount of iron oxides. The iron mainly formed in its zero valent (α -Fe) state with major reflections at 2 θ =44.91°(e1) and 2 θ =65.19°(e2). These peaks are weakened considerably, and iron oxide signals were detected in the XRD pattern of PCAC-Fe⁰ after reacting with nitrate ions (Figure 2f). In this pattern, three peaks at 2 θ =33.3° (f1), 35.8° (f2) and 62.9° (f3) were observed, which were assigned to the characteristic peaks of goethite (α -FeOOH), magnetite (Fe₃O₄) and maghemite (α -Fe₂O₃), respectively (Geng *et al.*, 2009).

It is evident that ZVI nanoparticles were acting as reducing agents, and the redox reaction has occurred between Fe⁰ and nitrate ions. PC-Fe⁰ and PCAC-Fe⁰ had typical PC and PCAC structures, respectively, indicated that PC and PCAC frameworks, and their total crystalline structures were not significantly changed after immobilizing ZVI nanoparticles. The calculated particle sizes (diameter) of PC-Fe⁰ and PCAC-Fe⁰ computed by the Scherrer equation (Birks and Friedman, 1946) were found to be 75 and 35 nm, respectively, which were in a good agreement with

the sizes determined by SEM images. FTIR technique gives information about the vibrational state of the adsorbed molecules; hence, FT-IR measurements were carried out to identify the stabilization mechanisms. FTIR spectra were recorded in the transmission mode between 500 and 4000 cm⁻¹ for all samples (Figure 3).

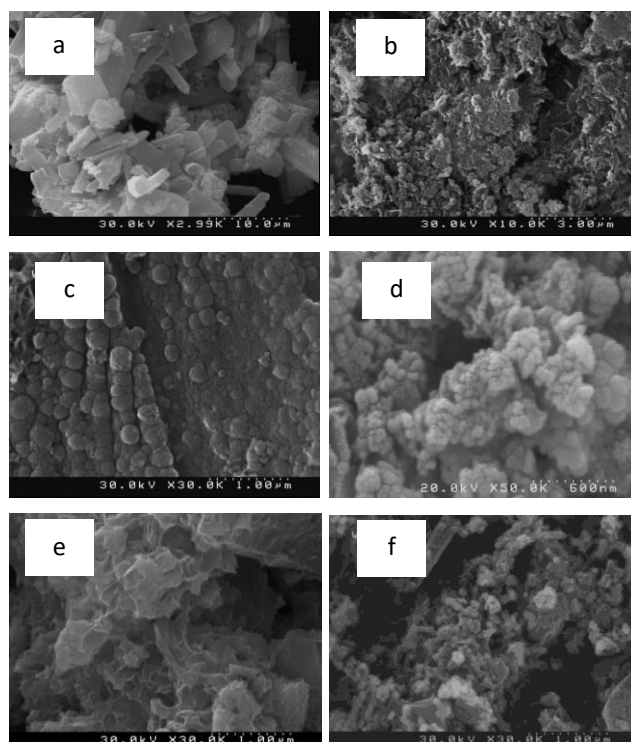


Figure 1. SEM images of: (a) PC, (b) PCAC, (c) PC-Fe⁰ and (d) PCAC-Fe⁰ before reacting with nitrate, (e) PC-Fe⁰ and (f) PCAC-Fe⁰ after reaction with nitrate

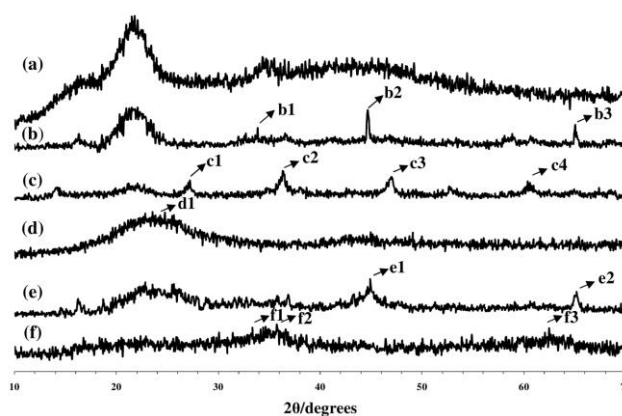


Figure 2. XRD patterns of (a) PC; (b) PC-Fe⁰ before reacting with nitrate; (c) PC-Fe⁰ after reacting with nitrate; (d) PCAC; (e) PCAC-Fe⁰ before reacting with nitrate; (f) PCAC-Fe⁰ after reacting with nitrate

The main absorption bands of PC were at the following wavelengths (Figure 3a): (1) 1040 cm⁻¹ generated by OH bending vibration and C-O-C stretching vibration, (2) 1220-1300 cm⁻¹ mainly attributed to the phase combination of C-N stretching, N-H bending vibrations (amide III region), (3) 1325-1410 cm⁻¹ assigned to the symmetric bending vibration of CH₃ and CH₂, and the shear-type vibration absorption of CH₃ in proteins and

cellulose (Amir *et al.*, 2004), (4) 1410-1450 cm^{-1} represented the C–O stretching vibration in carboxylate ions ($-\text{COO}-$), (5) 1450-1480, 2850, and 2920 cm^{-1} represented the symmetric and asymmetric stretching vibration of the CH_2 and CH_3 , (6) 1510-1530 cm^{-1} associated to the presence of N–H and C–H bending and stretching vibration (amide II region), (7) the amide I peak appeared at 1610-1650 cm^{-1} (Deng *et al.*, 2013), (8) 1734 cm^{-1} assigned to the C=O stretching vibration, and (9) 3000-3800 cm^{-1} attributed to the presence of –OH and –NH stretching vibration of carbohydrate, cell wall compounds, and proteins. The spectrum of PCAC (Figure 3c) reveals bands centered at 700-900 cm^{-1} attributed to the aromatic C–H stretching vibration. The band centered at 1145 cm^{-1} can be assigned to the aromatic CO– stretching vibration. The presence of band at 1560 cm^{-1} can be assigned to the aromatic C=C ring stretching. The peak at 2315 cm^{-1} was attributed to the C=O stretching (Kazemipour *et al.*, 2008). The band centered at 1705 cm^{-1} was assigned to the aromatic carboxyl C=O stretching vibration in ketones or carbonyl group (Tangjuank *et al.*, 2009), while the bands at 2850 and 2920 cm^{-1} were disappeared. The decreasing of the intensity of the peaks between 3300-3500 cm^{-1} pointed out the loss of surface-bonded moisture and decomposition of the cellulose-based pine cone structure.

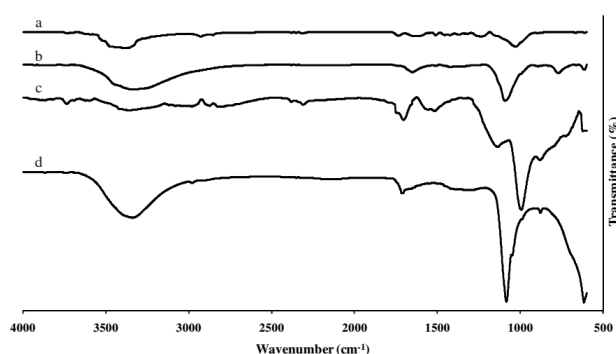


Figure 3. FTIR spectra of (a) PC, (b) PC-Fe⁰, (c) PCAC and (d) PCAC-Fe⁰

It can be observed that in Figures 3b and 3d, several noticeable changes are occurred in the spectrums of PC-Fe⁰ and PCAC-Fe⁰ in comparison with the spectrums of PC and PCAC. Plant cells are made of polysaccharide, protein, lipid composition, containing carbonyl, hydroxyl, carboxyl, amino and other active sites which could bind with iron ions (Ponder *et al.*, 2000; Macfie and Welbourn, 2000). In the case of PC-Fe⁰, the absorption peaks of carboxyl (1410-1450 cm^{-1}), amide (1220-1300; 1510-1530 and 1610-1650 cm^{-1}), and hydroxyl (3000-3800 cm^{-1}) groups were shifted significantly. Amide absorption bands were characteristics of protein spectra, so it can be reasonably supposed that proteins could chelate with iron ions, which was evidenced by other researchers (Arshadi *et al.*, 2014). The peaks at 2850 and 2920 cm^{-1} (CH_2 groups) were weakened in the spectrum of PC-Fe⁰. The IR band at 620 cm^{-1} is related to Fe–O stretching vibrations, also the weak band at 780 cm^{-1} is appeared

due to Fe–O–H bending vibrations in goethite (Gotic and Music, 2007). These peaks are only recognized in the spectrum of PC-Fe⁰, which is in a good agreement with the XRD pattern (Figure 2b), where the surface of the supported nZVI particles was partially oxidized. Compared to the FTIR spectra of PCAC (Figure 3c), changes in the adsorption peaks from PCAC-Fe⁰ in Figure 3d were observed. On the basis of IR bands (Figure 3d), strong adsorption peak at 3345 cm^{-1} (the stretching vibrations of the hydroxyl group) and adsorption peak at 1705 cm^{-1} (the stretching vibrations of the carboxylic group) are very sensitive to the stabilization of nZVI, and this bands are shifted significantly. A relative decrease in the carboxylic band and an increase in the OH band were recorded, indicating that these bands were affected due to the iron attachment which was evidenced by other researchers (Chen *et al.*, 2011; Li *et al.*, 2010; Li *et al.*, 2011a). In accordance with achievements by Gotic and Music (2007), the IR band at 618 cm^{-1} is related to Fe–O stretching vibrations (Gotic and Music, 2007). These results demonstrated that nZVI particles had been successfully loaded onto PCAC.

3.2. Effect of the initial pH and zeta potential

The effect of pH on the adsorption of nitrate by the adsorbents was studied over a pH range of 2-10 (Figure 4). The alteration of the surface charges as a function of pH (1.5-12.5) was measured in a 10^{-3} M NaCl background solution (Figure 5). At $\text{pH} < \text{pH}_{\text{pzc}}$ value of point of zero charge (pH_{pzc}), the sorbent has the positive surface charge, while at $\text{pH} > \text{pH}_{\text{pzc}}$, the surface charge of the sorbent is negative. It can be seen (Figure 4) that the nitrate removal was highly dependent on the initial pH of the solution. At higher pH, the competition for active sites by OH^- ions and the electrostatic repulsion of anionic nitrate by the negatively charged surface of the PC and PCAC may be resulted in less nitrate adsorption. Nitrate reduction by PCAC-Fe⁰ was observed to be higher compared to other adsorbents. PC-Fe⁰ and PCAC-Fe⁰ are more sensitive to the initial pH of solution than PC and PCAC. In the cases of PC-Fe⁰ and PCAC-Fe⁰, the removal efficiencies have a decreasing trend, when the initial pH is increased. A plausible explanation is that, at higher pH, Fe(II) and Fe(III) precipitation was gradually formed which covered the shell of ZVI nanoparticles, and subsequently reduced the degradation of nitrate (Liu *et al.*, 2012). Therefore, in lower pH, the Re (%) was increased significantly, and the maximum nitrate removal was occurred at $\text{pH}=2$, which had also been reported in other studies (Kassaeia *et al.*, 2011). The pH_{pzc} of PC is 4.5, while it decreases to 4 for PCAC (Figure 5). This phenomenon displayed that the activation of PC leads to a negatively charged surface of PCAC due to the separation of carboxyl functional groups (Malik *et al.*, 2002). After being modified with nZVI, the pH_{pzc} of PC and PCAC have been shifted to 6.8 and 6.45, respectively. Pure nZVI has zero point charges in the pH range 8-9 (Zhang, 2003). In comparison with the pH_{pzc} of pure nZVI, the determined pH_{pzc} of PC-Fe⁰ and PCAC-Fe⁰ samples are lower than that of the pure nZVI, which might

be due to the introduction of several oxygen-containing functional groups. The pH_{pzc} of PC-Fe⁰ and PCAC-Fe⁰ could propose an advantage for the removal of anions under neutral pH.

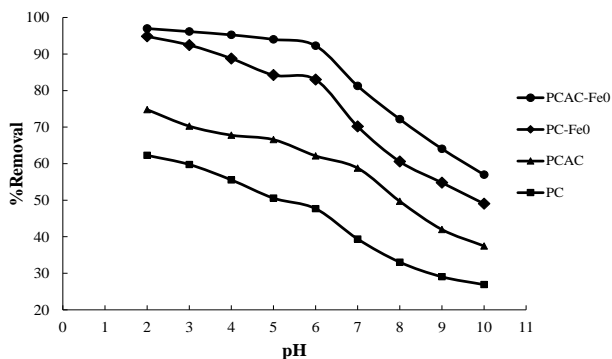


Figure 4. Effect of pH on the nitrate adsorption by PC, PCAC, PC-Fe⁰ and PCAC-Fe⁰ ($C_0=100 \text{ mg L}^{-1}$, sorbent dosage= 10 g L^{-1} , $T=25 \text{ }^\circ\text{C}$)

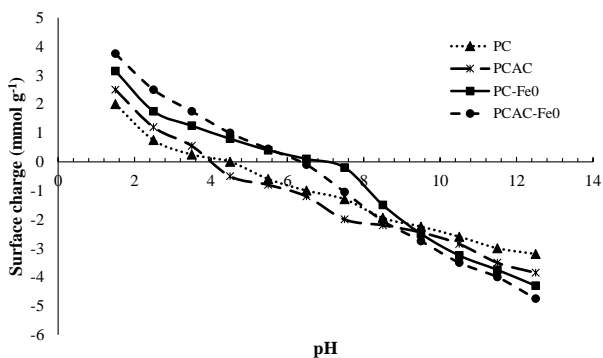


Figure 5. Zeta potential of the sorbents as a function of pH
Experimental error: $\pm 4 \text{ mV}$

3.3. Effect of the sorbent dosage and adsorption temperature

The initial loadings of adsorbents in the nitrate solution were 2-10 (g L^{-1}). The initial nitrate concentration and the initial pH value of the solutions were adjusted at 100 (mg L^{-1}) and 6, respectively. The removal efficiencies (%) were increased as the sorbent dosages were increased (Figure 6). As the adsorbents dosages increased from 2 to 6 (g L^{-1}), the removal efficiencies of nitrate ions increased significantly from 58.9% to 76.1% and 65.2% to 87.2% for PC-Fe⁰ and PCAC-Fe⁰, respectively. This phenomenon can be attributed to the increase in the available adsorption sites and bigger surface area with the increase in the sorbent dosage. With a further increase in sorbent dosages to 10 (g L^{-1}), the nitrate removal is increased slightly to 83 and 92.3% for PC-Fe⁰ and PCAC-Fe⁰, respectively. This was because of the saturation of the active sites (Shi *et al.*, 2011). Figure 7 demonstrates the effect of adsorption temperature (25-55 $^\circ\text{C}$) on the removal efficiency of nitrate ions ($C_0=100 \text{ mg L}^{-1}$, $pH=6$). It can be seen from Figure 7 that the removal percentage of nitrate increased with an increase in the adsorption temperature from 25 to 55 $^\circ\text{C}$. This might be because of

high temperature is beneficial for the diffusion of nitrate ions to active adsorption sites of adsorbents, which will favor the adsorption of nitrate. Therefore, in higher temperature, the Re(%) was increased slightly, and the maximum nitrate removal percentage (Re= 97%) was belong to PCAC-Fe⁰ at $T= 55 \text{ }^\circ\text{C}$, which is in accordance with the other studies (Song *et al.*, 2016; Tong *et al.*, 2017).

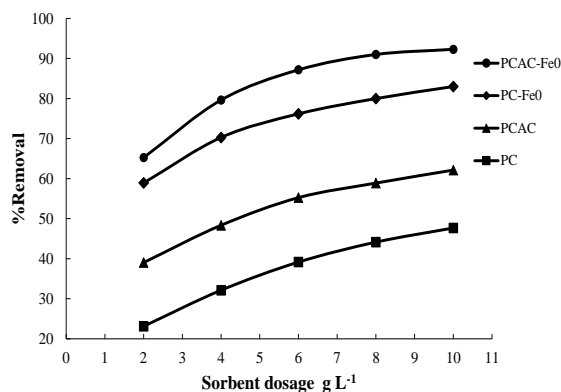


Figure 6. The variation of nitrate adsorption (%) at different sorbent dosages, $pH=6$, $T=25 \text{ }^\circ\text{C}$

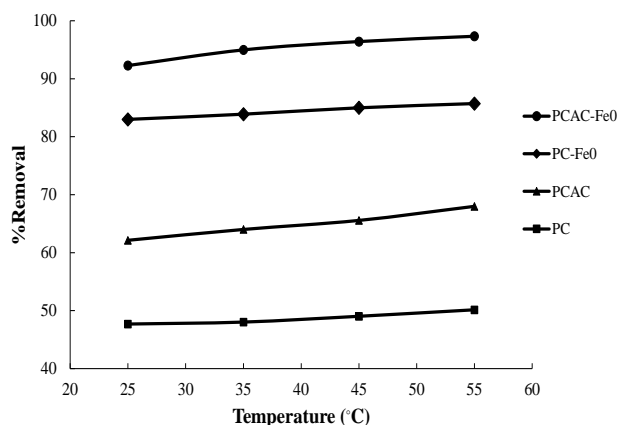


Figure 7. Effect of the adsorption temperature on the nitrate adsorption by PC, PCAC, PC-Fe⁰ and PCAC-Fe⁰

3.4. Fate of nitrogen species during nitrate reduction by PC-Fe⁰ and PCAC-Fe⁰

In the experiments with PC-Fe⁰ and PCAC-Fe⁰, the concentrations of ammonium, nitrite and nitrate, accumulated in the solution at every time interval, were determined at initial $pH=6$, $T=25 \text{ }^\circ\text{C}$ and $C_0=100 \text{ mg L}^{-1}$. Moreover the mass of ammonium sorbed on PC-Fe⁰ and PCAC-Fe⁰ was measured by extracting with 1.0 M KCl solution and analyzing the extract solution. The concentrations of nitrogen species during the nitrate reduction by PC-Fe⁰ and PCAC-Fe⁰ are presented in Figures 8 and 9. At the end of the reaction period, the $\text{NH}_4^+\text{-N}$ concentrations extracted from PC-Fe⁰ and PCAC-Fe⁰ were accounted for about 72.7% and 82.1% of the nitrate reduced, respectively (Figures 8 and 9). The total amount of nitrogen species (TN) in PCAC-Fe⁰ and PC-Fe⁰ systems were calculated as the sum of three main

aqueous nitrogen species (ammonium, nitrate and nitrite) and NH_4^+ extracted from PCAC and PC, after the reduction reaction was carried out for 24 h. In the case of PCAC- Fe^0 , the NH_4^+ concentration in the solution phase was undetectable at every time interval, indicating that the ammonium produced from nitrate reduction, completely was sorbed on PCAC- Fe^0 . PC- Fe^0 releases little ammonium in the residual solution (about 15.3% of the nitrate reduced), which is unfavorable. The TN decreased to 11.1% and 10.6% of the initial nitrate concentration in PC- Fe^0 and PCAC- Fe^0 systems, respectively. This phenomenon is probably due to the nitrogen conversion from aqueous phase to gas phase. This result agreed with the results of other researchers (Hwang *et al.*, 2011; Shi *et al.*, 2013). It was experimentally proven that the role of nZVI in the removal of nitrate should be taken part in two major processes: (I) adsorption of nitrate on the nZVI surface; (II) directly participation in the redox reaction (Hwang *et al.*, 2011). This result is pointed out by several authors for the removal of a variety of contaminants using nZVI including: Cr (VI) (Geng *et al.*, 2009), As(III) (Horzum *et al.*, 2013), NO_3^- (Hwang *et al.*, 2011; Rodriguez *et al.*, 2009.), Cu^{2+} , Co^{2+} (Uzum *et al.*, 2009), pentachlorophenol (Li *et al.*, 2011b), and methyl orange (Chen *et al.*, 2011).

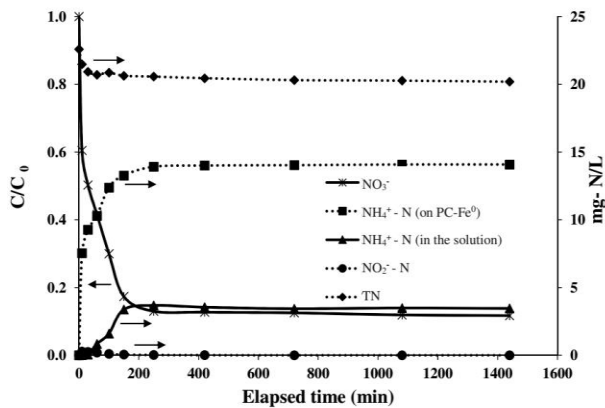


Figure 8. Total nitrogen, ammonium, nitrate and nitrite concentrations in the residual solution and ammonium extracted from PC- Fe^0 after reaction

3.5. Adsorption kinetics

The rate of adsorption of nitrate was studied at initial pH=6 and T=25°C ($C_0=100 \text{ mg L}^{-1}$) up to a contact time 24 h. The experimental data were fitted to the kinetic models (Pseudo-first-order, Pseudo second-order and Intra-particle diffusion) by the nonlinear regression analysis using GraphPad Prism tool. Mentioned models are described by Eqs. (4)-(6):

$$\text{Pseudo-first-order: } q_t = q_e (1 - e^{-k_1 t}) \quad (4)$$

$$\text{Pseudo-second-order: } q_t = \frac{k_2 q_e^2 t}{1 + k_2 q_e t} \quad (5)$$

$$\text{Intra-particle diffusion: } q_t = k_i t^{0.5} - C \quad (6)$$

Where q_t and q_e are the amounts of the nitrate ions sorbed by adsorbents at time t (min) and at equilibrium condition (mg g^{-1}), respectively, and k_1 , k_2 , k_i and C are constants.

The initial adsorption rate, h , ($\text{mg g}^{-1} \text{ min}^{-1}$) is expressed as:

$$h = k_2 q_e^2 \quad (7)$$

The application of the kinetic models on experimental results is presented in Figure 10. The kinetic parameters, the correlation coefficients (R^2) and the Standard Error of Estimate (SEE) values for nitrate sorption by adsorbents are given in Table 3. A higher R^2 and a lower SEE, indicate a better matching between the experimental (exp) and calculated (cal) nitrate sorption data. In all cases, nitrate adsorption data were fitted well to the Pseudo second-order model, as indicated by the higher R^2 and lower SEE values (Table 3).

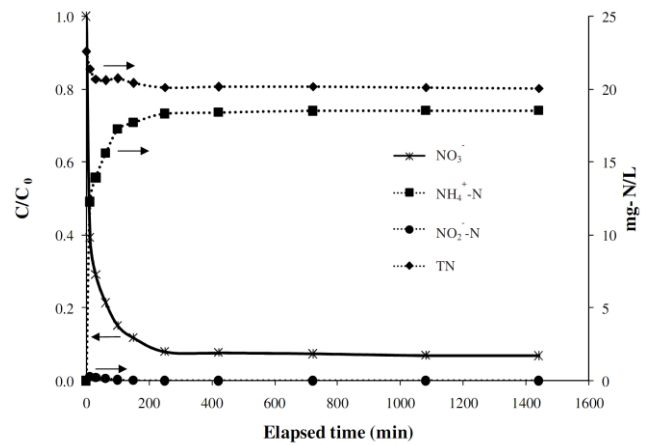


Figure 9. Total nitrogen, nitrate and nitrite concentrations in residual solution and ammonium extracted from PCAC- Fe^0 after reaction

On the other hand, as shown in Table 3, it is noticed that PCAC- Fe^0 has the highest initial adsorption rate ($h=1.4124$). Thus, PCAC- Fe^0 reacted with nitrate ions much faster than the other samples under the same conditions. Figure 10 shows that the kinetic of the nitrate adsorption includes two phases. Phase I: an initial phase with the rapid rise of the adsorption rate, and Phase II: a gradual adsorption second phase, when adsorption reaches the equilibrium condition. The initial high rate of nitrate removal (Phase I) can be attributed to the most readily available binding sites on the sorbent surfaces (Chatterjee and Woo, 2009). Phase II may be attributed to the slow diffusion of the nitrate from the surface sites into meso- or micro pores. As a result, nitrate uptake occurs both on the surface/pores on the sorbents.

3.6. Adsorption isotherm

In order to evaluate the adsorption capacities of the adsorbents for nitrate, sets of experiments were conducted at various initial concentrations (20-320 mg L^{-1}). Equilibrium adsorption data were analyzed using

Langmuir, Freundlich and Langmuir-Freundlich isotherm models, described by Eqs. (8)-(10):

$$\text{Langmuir model: } q_e = \frac{q_m k_l C_e}{1 + k_l C_e} \quad (8)$$

$$\text{Freundlich model: } q_e = k_f C_e^n \quad (9)$$

$$\text{Langmuir-Freundlich model: } q_e = \frac{q_m k_l C_e^{1/n}}{1 + k_l C_e^{1/n}} \quad (10)$$

Where q_e (mg g^{-1}) and C_e (mg L^{-1}) are the amounts of adsorbed nitrate per unit mass of adsorbent at equilibrium condition and equilibrium concentration of nitrate in the solution, respectively. q_m (mg g^{-1}) is the maximum adsorption capacity. k_l (L mg^{-1}), k_f (L g^{-1}) and n are constants. The dimensionless constant separation factor (R_L) can be used to determine whether the adsorption is favorable or not. R_L is given by the following equation:

Table 3. Parameter of the kinetic models for the adsorption of nitrate onto PC, PCAC, PC-Fe⁰ and PCAC-Fe⁰

Adsorbent		PC	PC-Fe ⁰	PCAC	PCAC-Fe ⁰
Pseudo first-order	q_e (exp) (mg g^{-1})	5.154	8.827	6.467	9.314
	q_e (cal) (mg g^{-1})	4.992	8.534	6.081	8.833
	k_1 (L mg^{-1})	0.007	0.267	0.033	0.097
	R^2	0.931	0.803	0.851	0.755
	SEE	0.429	0.867	0.521	0.698
Pseudo second-order	q_e (cal) (mg g^{-1})	5.567	8.986	6.452	9.224
	k_2 (L mg^{-1})	0.002	0.005	0.008	0.016
	h ($\text{mg g}^{-1} \text{min}^{-1}$)	0.558	0.345	0.428	1.412
	R^2	0.959	0.921	0.964	0.925
	SEE	0.327	0.547	0.254	0.324
Intra-particle diffusion	k_i ($\text{mg g}^{-1} \text{min}^{-0.5}$)	0.121	0.123	0.087	0.072
	C	-1.330	-5.261	-3.862	-7.202
	R^2	0.884	0.636	0.664	0.602
	SEE	0.554	0.776	0.784	0.749

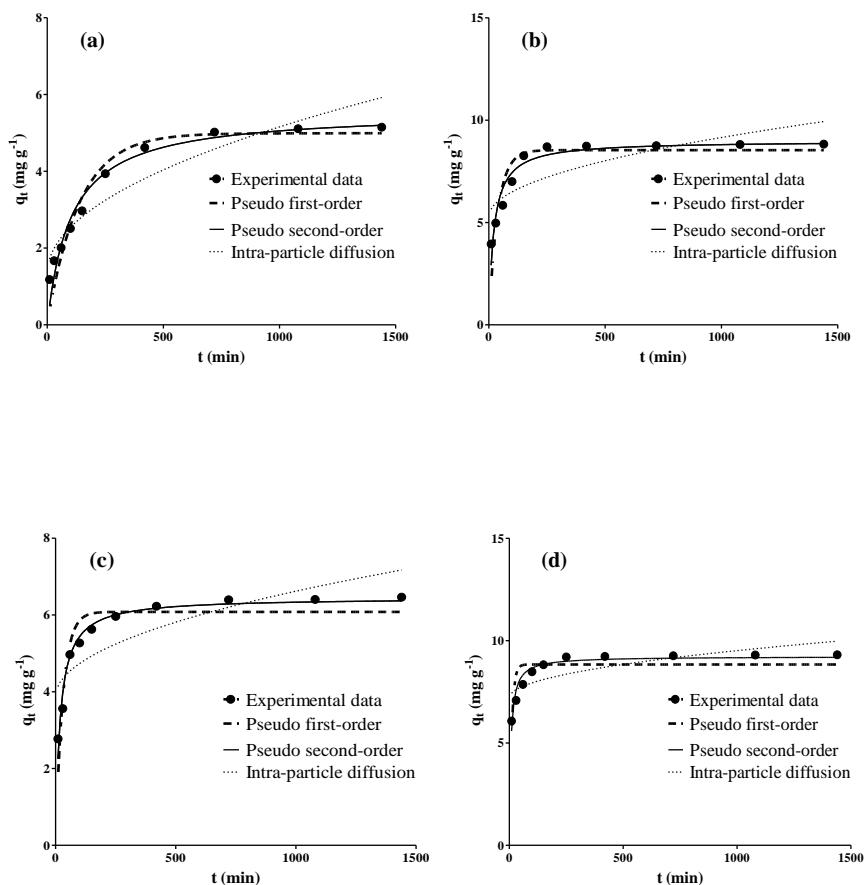


Figure 10. Nitrate adsorption kinetics by (a) PC, (b) PC-Fe⁰, (c) PCAC, and (d) PCAC-Fe⁰

$$R_L = \frac{1}{1 + K_f C_0} \quad (11)$$

If $R_L > 1$, the adsorption is unfavorable; when $R_L = 0$, the adsorption is irreversible; when $R_L = 1$, the adsorption is linear; in the range $0 < R_L < 1$, the adsorption is favorable (Ozcan and Ozcan, 2009). The isotherm parameters, R^2 and SEE values for nitrate sorption by adsorbents are given in Table 4. The application of the isotherm models on experimental results is presented in Figure 11. In all cases, comparing R^2 and SEE values (Table 4) demonstrated that the experimental data were well

fitted to the Langmuir-Freundlich model. This means that sorption takes place at the functional group/binding sites on the surface of the sorbents. Figure 11 illustrates that the nitrate adsorption capacities of the all adsorbents is firstly increased with increasing the initial concentration of nitrate, and then they are not changed significantly, indicating that no more sites remain available for adsorption. The maximum adsorption capacities of the PC-Fe⁰ and PCAC-Fe⁰ for nitrate are 18.16 and 22.30 (mg g⁻¹), respectively. According to the value of R_L (Table 4), the adsorption of nitrate onto the all adsorbents is favorable.

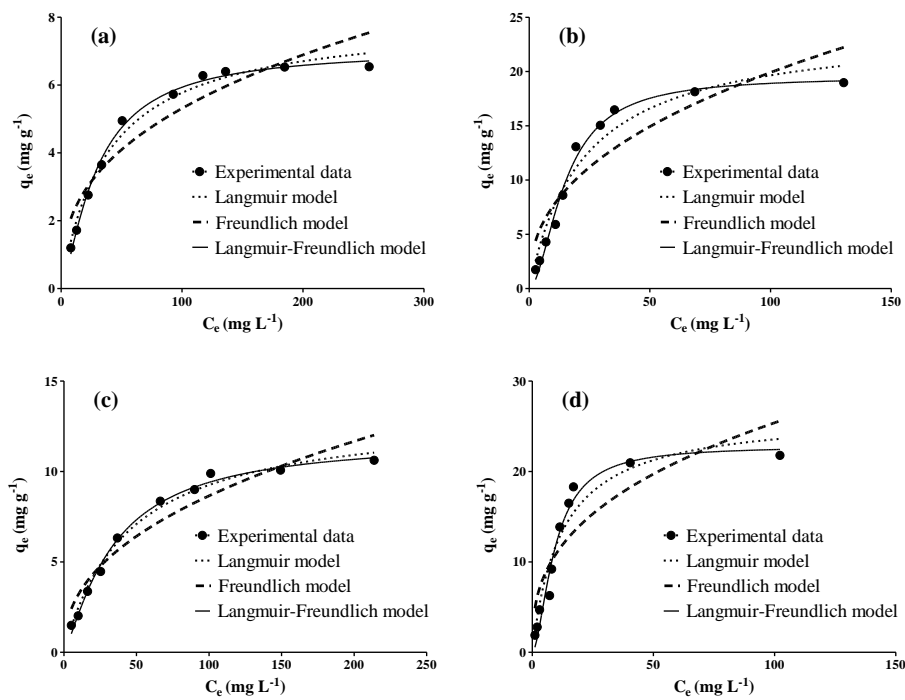


Figure 11. Isotherm plots for the adsorption of nitrate ions onto (a) PC, (b) PC-Fe⁰, (c) PCAC and (d) PCAC-Fe⁰

Table 4. Isotherm parameters for the adsorption of nitrate onto PC, PCAC, PC-Fe⁰ and PCAC-Fe⁰

Adsorbent	Isotherm	PC	PC-Fe ⁰	PCAC	PCAC-Fe ⁰
Langmuir	q_m (mg g ⁻¹)	7.991	24.09	13.31	26.40
	k_f (Lmg ⁻¹)	0.026	0.044	0.023	0.083
	R_L	0.087-0.752	0.108-0.857	0.102-0.826	0.134-0.936
	R^2	0.985	0.950	0.789	0.938
	SEE	0.272	0.573	0.383	0.404
Freundlich	k_f (L mg ⁻¹)	0.944	2.933	1.186	4.732
	n	2.665	2.404	2.317	2.742
	R^2	0.897	0.830	0.925	0.798
	SEE	0.710	0.901	0.517	0.619
Langmuir-Freundlich	k_f (Lmg ⁻¹)	0.009	0.007	0.012	0.022
	q_m	6.84	18.16	11.07	22.30
	n	0.734	0.557	0.802	0.585
	R^2	0.951	0.993	0.975	0.989
	SEE	0.355	0.192	0.210	0.201

4. Conclusion

In this study, nZVI particles supported on raw pine cone (PC-Fe⁰) and pine cone activated carbon (PCAC-Fe⁰) were synthesized, characterized, and applied for the removal of nitrate as a model contaminant from aqueous solution. These novel materials have high specific surface area, and based on the SEM results, nZVI particles are uniformly dispersed across PC and PCAC surface without noticeable aggregation. Natural waste materials are low-cost sorbents, thus, these materials could be effective and promising stabilizers, and dispersants for supporting nZVI particles due to their porous structures. Batch experiments indicated that the nitrate removal efficiency decreased with increasing the initial concentration of nitrate and initial pH but increased with increasing in the sorbent dosages and temperature. The maximum adsorption capacities of PC-Fe⁰ and PCAC-Fe⁰ for nitrate were 18.16 and 22.30 (mg g⁻¹), respectively. Reduction of nitrate using PC-Fe⁰ and PCAC-Fe⁰ was in accordance with the pseudo second order kinetic model. Moreover, the equilibrium data were fitted well to the Langmuir-Freundlich model. These novel composites are effective at the neutral pH of the solution (pH=6) without any pH adjustment. The nitrogen mass balance calculation revealed that nZVI particles in PC-Fe⁰ and PCAC-Fe⁰ beads could generally reduce nitrate into ammonium (more than 72% and 82% of the reduced nitrate, for PC-Fe⁰ and PCAC-Fe⁰, respectively), and nitrite usually occurs as intermediate. Subsequently, PCAC-Fe⁰ absorbs completely un-wanted ammonium due to its high surface area. PC-Fe⁰ has less sorption capacity for ammonium in comparison with PCAC-Fe⁰. PC-Fe⁰ releases little ammonium in the residual solution (about 15.3% of the reduced nitrate), which is unfavorable. It is concluded that the nitrate removal using PC-Fe⁰ and PCAC-Fe⁰ consists of three steps: 1) the adsorption of nitrate on the nZVI surface; 2) the redox reaction between nZVI and nitrate ions; 3) the ammonium absorption by PC-Fe⁰ and PCAC-Fe⁰. In view of this, PCAC-Fe⁰, as a low-cost nano-biocomposite, has a great potential to be used as an economical and efficient adsorbent to remove nitrate from water and wastewater.

References

- Allaf R.M., Rivero I.V., Speraman S.S. and Hope-Weeks J. (2011), On the preparation of as-produced and purified single-walled carbon nanotube samples for standardized X-ray diffraction characterization. *Materials Characterization*, **62**(9), 857-864.
- Amir S., Hafidi M., Merlina G., Hamdi H. and Revel J.C. (2004), Elemental analysis, FTIR and ¹³C-NMR of humic acids from sewage sludge composting. *Agronomie*, **24**(1), 13-18.
- APHA W. (1992) *Standard Methods for the Examination of Water and Wastewater*. Am. Public Health Assoc. Washington, DC.
- Arshadi M., Soleymanzadeh M., Salvacion J.W.L. and SalimiVahid F. (2014), Nanoscale zerovalent iron supported on siniguelas waste for the removal of Pb(II) ions from aqueous solution. *Journal of Colloid and Interface Science*, **426**, 241-251.
- Birks L.S. and Friedman H. (1946), Particle size determination from X-ray line broadening. *Journal of Applied Physics*, **16**, 687-692.
- Bossa N., Carpenter A., Kumar N., Lannoy C. and Wiesner M. (2017), Cellulose nanocrystal zero-valent iron nanocomposites for groundwater remediation. *Environmental Science: Nano*, **4**(6), 1294-1303.
- Chatterjee S. and Woo S.H. (2009), The removal of nitrate from aqueous solutions by chitosan hydrogel beads. *Journal of Hazardous Materials*, **164**, 1012-1018.
- Chen Z.X., Jin X.Y., Chen Z. and Megharaj M. (2011), Removal of methyl orange from aqueous solution using bentonite-supported nanoscale zero-valent iron. *Journal of Colloid and Interface Science*, **363**, 601-607.
- Deng P.Y., Liu W., Zeng B.Q., Qiu Y.K. and Li L.S. (2013), Sorption of heavy metals from aqueous solution by dehydrated powders of aquatic plants. *International Journal of Environmental Science and Technology*, **10**, 559-566.
- Driscoll C., Whittall D., Aber J., Boyer E., Castro M., Cronan C., Goodale C., Groffman P., Hopkinson C., Lambert K., Lawrence G. and Ollinger S. (2003), Nitrogen pollution: sources and consequences in the U.S. Northeast. *Environment: Science and Policy for Sustainable Development*, **45**(7), 8-22.
- Geng B., Jin Z., Li T. and Qi X. (2009), Preparation of chitosan-stabilized Fe⁰ nanoparticles for removal of hexavalent chromium in water. *Science of the Total Environment*, **407**(18), 4994-5000.
- Gotic M. and Music S. (2007), Mossbauer, FTIR and FE SEM investigation of iron oxides precipitated from FeSO₄ solutions. *Journal of Molecular Structure*, **834**, 445-453.
- Haykiri H., Yaman S. and Kucukbayrak S. (2010), Effect of biomass on temperatures of sintering and initial deformation of lignite ash. *Fuel*, **89**, 3063-3068.
- Horzum N., Demir M., Nairat M. and Shahwan T. (2013), Chitosan fiber-supported zero-valent iron nanoparticles as a novel sorbent for sequestration of inorganic arsenic. *RSC Advances*, **3**, 7828-7837.
- Hou M., Wan H., Liu T., Fan Y., Liu X. and Wang X. (2008), The effect of different divalent cations on the reduction of hexavalent chromium by zerovalent iron. *Applied Catalysis B: Environmental*, **84**(1), 170-175.
- Huang D., Xue W., Zeng G., Wan J., Chen G., Huang C., Zhang C., Cheng M. and Xu P. (2016), Immobilization of Cd in river sediments by sodium alginate modified nanoscale zero-valent iron: Impact on enzyme activities and microbial community diversity. *Water Research*, **106**, 15-25.
- Hwang Y.H., Kim D.G. and Shin H.S. (2011), Mechanism study of nitrate reduction by nano zero valent iron. *Journal of Hazardous Materials*, **185**, 1513-1521.
- Joo S.H. and Zhao D. (2008), Destruction of lindane and atrazine using stabilized iron nanoparticles under aerobic and anaerobic conditions: Effects of catalyst and stabilizer. *Chemosphere*, **70**, 418-425.
- Kassae M.Z., Motamedi E., Mikhak A. and Rahnemaie R. (2011), Nitrate removal from water using iron nanoparticles produced by arc discharge vs. reduction. *Chemical Engineering Journal*, **166**, 490-495.
- Kazempour M., Ansari M., Tajrobehkar S., Majdzadeh M. and Reihani-Kermani H. (2008), Removal of lead, cadmium,

- zinc, and copper from industrial wastewater by carbon developed from walnut, hazelnut, almond, pistachio shell, and apricot stone. *Journal of Hazardous Materials*, **150**, 322-327.
- Keeney D.R. and Nelson D.W. (1982) *Nitrogen Inorganic Forms, Methods of Soil Analysis, Part 2*. second ed. SSSA. Madison, Agronomy ASA, pp. 643-698.
- Kim H., Kapwn D., Mayer B., Lee J., Hyun Y. and Lee K. (2015), Identifying the sources of nitrate contamination of groundwater in an agricultural area (Haeon basin, Korea) using isotope and microbial community analyses. *Science of the Total Environment*, **533**, 566-575.
- Li S., Wu P., Li H., Zhu N., Li P., Wu J., Wang X. and Dang Z. (2010), Synthesis and characterization of organo-montmorillonite supported iron nanoparticles. *Applied Clay Science*, **50**, 330-338.
- Li Y., Li T. and Jin Z. (2011a), Stabilization of Fe⁰ nanoparticles with silica fume for enhanced transport and remediation of hexavalent chromium in water and soil. *Journal of Environmental Sciences*, **23**(7), 1211-1218.
- Li Y., Zhang Y., Li J. and Zheng X. (2011b), Enhanced removal of pentachlorophenol by a novel composite: Nanoscale zero valent iron immobilized on organobentonite. *Environmental Pollution*, **159**, 3744-3749.
- Lin Y.T., Weng C.H. and Chen F.Y. (2008), Effective removal of AB24 dye by nano/micro-size zero-valent iron. *Separation and Purification Technology*, **64**, 26-30.
- Liu T., Wang Z.L., Zhao L. and Yang X. (2012), Enhanced chitosan/Fe⁰-nanoparticles beads for hexavalent chromium removal from wastewater. *Chemical Engineering Journal*, **189-190**, 196-202.
- Lomnicki S. and Dellinger B. (2003), Development of supported iron oxide catalyst for destruction of PCDD/F. *Environmental Science and Technology*, **37**, 4254-4260.
- Macfie S.M. and Welbourn P.M. (2000), The cell wall as a barrier to uptake of metal ions in the unicellular green alga *Chlamydomonas reinhardtii* (Chlorophyceae). *Archives of Environmental Contamination and Toxicology*, **39**(4), 413-419.
- Malik D.J., Streiko V., Streat M. and Puizy A.M. (2002), Characterisation of novel modified active carbons and marine algal biomass for the selective adsorption of lead. *Water Research*, **36**, 1527-1538.
- Mukherjee R., Kumar R., Sinha A., Lama Y. and Saha A. (2016), A review on synthesis, characterization, and applications of nano zero valent iron (nZVI) for environmental remediation. *Critical Reviews in Environmental Science and Technology*, **46**(5), 443-466.
- Ozcan S.A. and Ozcan O. (2009), Adsorption of lead(II) ions onto 8-hydroxy quinoline-immobilized bentonite. *Journal of Hazardous Materials*, **161**, 499-509.
- Pan G., Li L., Zhao D. and Chen H. (2010), Immobilization of non-point phosphorus using stabilized magnetite nanoparticles with enhanced transportability and reactivity in soils. *Environmental Pollution*, **158**, 35-40.
- Ponder S.M., Darab J.G. and Mallouk T.E. (2000), Remediation of Cr (IV) and Pb(II) aqueous solutions using supported, nanoscale zero-valent iron. *Environmental Science and Technology*, **34**, 2564-2569.
- Rodriguez J.M., Garcia F., Garcia A., Gomez C. and Vereda C. (2009), Kinetics of the chemical reduction of nitrate by zero-valent iron. *Chemosphere*, **74**, 804-809.
- Shi J., Yi S., He H., Lomg C. and Li A. (2013), Preparation of nanoscale zero-valent iron supported on chelating resin with nitrogen donor atoms for simultaneous reduction of P Pb²⁺ and NO₃⁻. *Chemical Engineering Journal*, **230**, 166-171.
- Shi L., Zhang X. and Chen Z.L. (2011), Removal of Cr (VI) from wastewater using bentonite-supported nanoscale zero-valent iron. *Water Research*, **45**, 886-892.
- Song W., Gao B., Wang F., Xue N., Sun S., Song W. and Jia R. (2016), Adsorption of nitrate from aqueous solution by magnetic amine-crosslinked biopolymer based corn stalk and its chemical regeneration property. *Journal of Hazardous Materials*, **304**, 280-290.
- Sun S. and Zeng H. (2002), Size-Controlled synthesis of magnetite nano-particles. *Journal of the American Chemical Society*, **124**, 8240-8205.
- Tada K., Kawaguchi T. and Shimazu K. (2004), High electrocatalytic performance of Pd/Sn/Au electrodes for nitrate reduction. *Journal of Electroanalytical Chemistry*, **572**, 93-99.
- Tangjuank S., Insuk N., Tontrakoon J. and Udeye V. (2009), Adsorption of Lead(II) and Cadmium(II) ions from aqueous solutions by adsorption on activated carbon prepared from cashew nut. *World Academy of Science, Engineering and Technology*, **3**, 4-28.
- Tong X., Yang Z., Xu P., Li Y. and Niu X. (2017), Nitrate adsorption from aqueous solutions by calcined ternary Mg-Al-Fe hydrotalcite. *Water Science and Technology*, **75**(10), 2194-2203.
- Uzum C., Shahwan T., Eroglu A.E., Hallam K.R. and Scott T. (2009), Synthesis and characterization of kaolinite-supported zero-valent iron nanoparticles and their application for the removal of aqueous Cu²⁺ and Co²⁺ ions. *Applied Clay Science*, **43**, 172-181.
- Wang W., Zhou M., Mao Q., Yue J. and Wang X. (2010), Novel NaY zeolite-supported nanoscale zero-valent iron as an efficient heterogeneous Fenton catalyst. *Catalysis Communications*, **11**, 937-941.
- Wang X., Chen C., Liu H. and Ma J. (2008), Preparation and characterization of PAA/PVDF membrane-immobilized Pd/Fe nanoparticles for dechlorination of trichloroacetic acid. *Water Research*, **42**, 4656-4664.
- Wang X., Wang P., Ma J., Liu H. and Ning P. (2015), Synthesis, characterization, and reactivity of cellulose modified nano zero-valent iron for dye discoloration. *Applied Surface Science*, **345**, 57-66.
- Zhang W.X. (2003), Nanoscale iron particles for environmental remediation: an overview. *Journal of Nanoparticle Research*, **5**, 323-332.
- Zhao X., Liu W., Cai Z., Han B., Qian T. and Zhao D. (2016), An overview of preparation and applications of stabilized zero-valent iron nanoparticles for soil and groundwater remediation. *Water Research*, **100**, 245-266.